Journal Pre-proof

Effect of dislocation channeling and kink band formation on enhanced tensile properties of a new beta Ti alloy

S. Sadeghpour, S.M. Abbasi, M. Morakabati, L.P. Karjalainen

Please cite this article as: S. Sadeghpour, S.M. Abbasi, M. Morakabati, L.P. Karjalainen, Effect of dislocation channeling and kink band formation on enhanced 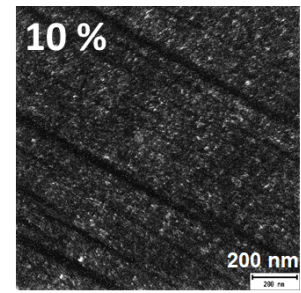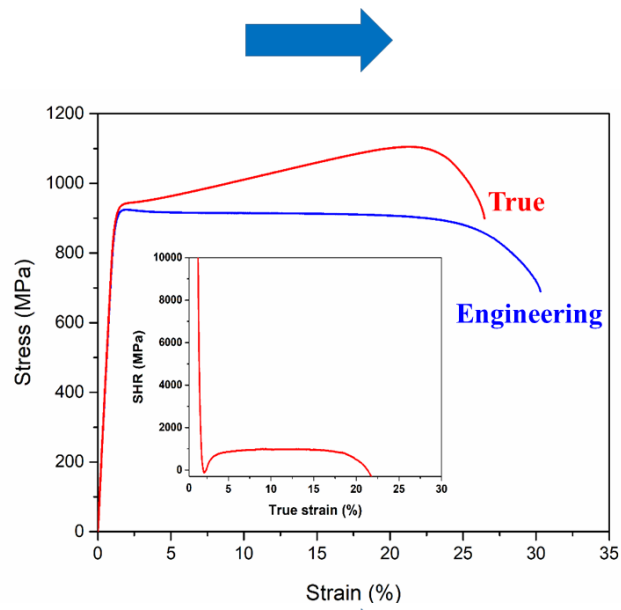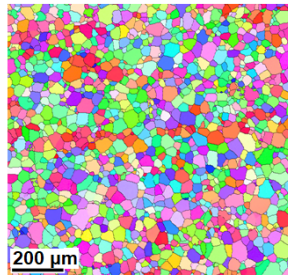tensile properties of a new beta Ti alloy, *Journal of Alloys and Compounds* (2019), doi: https://doi.org/10.1016/j.jallcom.2019.151741.

This is a PDF file of an article that has undergone enhancements after acceptance, such as the addition of a cover page and metadata, and formatting for readability, but it is not yet the definitive version of record. This version will undergo additional copyediting, typesetting and review before it is published in its final form, but we are providing this version to give early visibility of the article. Please note that, during the production process, errors may be discovered which could affect the content, and all legal disclaimers that apply to the journal pertain.
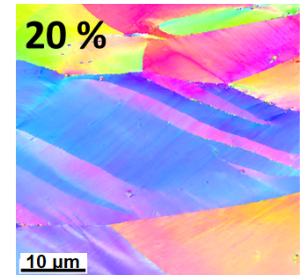
Effect of dislocation channeling and kink band formation on enhanced tensile properties of a new beta Ti alloy

S. Sadeghpour[a,b] [1], S.M. Abbasi[a], M. Morakabati[a], L.P. Karjalainen[b]

[a]Metallic Materials Research Center, Malek Ashtar University of Technology, Tehran, Iran

[b] Centre for Advanced Steels Research, University of Oulu, 90014 Oulu, Finland

Abstract

Tensile properties and deformation mechanisms of a newly developed β Ti alloy, Ti-3Al-8Mo-7V-3Cr (wt.%), were investigated at room temperature. The alloy was found to exhibit a yield point at high strength level of 920 MPa and excellent total elongation of 31%. The yield point was presumably caused by the oxygen in the alloy, although the nano-sized omega precipitates were present, too. The examinations of deformed microstructures at different strains using transmission electron microscope and electron backscatter diffraction showed that during straining dislocation glide occurred in narrow channels and kink bands were formed leading to a high ductility. The competing effect of strain hardening by intersecting of channels and twins and softening by kink band formation results in a flat plateau-type engineering stress-strain curve.

Keywords: Beta Ti alloy, yield strength, ductility, dislocation channels, kink band, strain hardening

1. Introduction

---

[1] Corresponding author, Tel.: +98 9369159669; E-mail: sinsad64@yahoo.com

Beta Ti alloys are being used in several applications including aerospace and medical industries. However, some drawbacks limit the extension of their usage in new applications. One of the most important drawbacks is the low ductility at room temperature preventing the production of the β Ti alloys in sheet form. In order to improve the ductility, Ti-Nb-Ta-Zr-O alloys, Gum metals, and some binary Ti-Mo alloys were developed and they may be considered as an initial suggestion for applications where the high cold workability was desired. Gum metals have attracted large attention during the past decade due to unconventional plasticity mechanism suggested for them [1]. The early studies claimed that these alloys deform by the formation of giant faults, which is a dislocation free mechanism [1, 2]. These observations were attributed to the low ideal shear strength of Gum metals [1, 3]. However, in recent years several researchers have reported conventional deformation mechanisms in Gum metals such as dislocation slip [4, 5], twinning [6, 7] and stress-induced martensitic transformation (SIMT) [8-10].

According to current knowledge, during deformation of β Ti alloys, several deformation mechanisms such as SIMT, mechanical twinning and dislocation slip or a combination of these may occur depending on the β phase stability [11]. Due to the importance of superelasticity and shape memory effects, SIMT has widely been investigated [12-14]. Two different twinning systems have been identified in β Ti alloys [15-17]. Contrary to this, there are few reports regarding dislocation slip and mobility in β Ti alloys. Only Castany et al. [4, 5, 18] have studied the slip behavior in TNTZO and TNTZSi alloys. They observed slip of screw dislocations during in situ tensile testing of a Gum metal in a transmission electron microscope and suggested the conventional dislocation slip as dominant deformation mechanism. It has been shown that β Ti alloys deforming predominantly by the twinning mechanism exhibit a high ductility [19, 20], whereas the alloys deforming by dislocation slip exhibit a high yield strength but very low

2

ductility [19]. This contradiction between the observed dislocation slip and the high ductility of Gum metals or other beta Ti alloys has rarely been addressed.

The present authors have recently introduced a new β Ti alloy (Ti-3873) with the nominal chemical composition Ti-3Al-8Mo-7V-3Cr (wt.%) showing a very high ductility during compressive deformation at room temperature [21]. This high plasticity is similar to that observed in Gum metals [22]. The present study aims to evaluate the tensile behavior of this new alloy and to understand the underlying deformation mechanism(s).

2. Materials and experimental methods

The alloy Ti-3873 with the chemical composition of Ti-2.9Al-7.9Mo-7V-3Cr-0.18O (wt. %) was produced by double melting in a vacuum arc furnace. After homogenizing for 4 h at 1100 °C and subsequent hot deformation, pieces from the plates were solution-treated at 1000 °C for 30 min followed by water quenching. The solution treated pieces were cold rolled at room temperature to reduce the thickness by 70%, revealing the high plasticity, and then annealed at 880 °C for 5 min and quenched in water. The annealing was carried out in β phase region, as the β transus temperature was determined by metallographic methods to be around 800 °C. The tensile test specimens were cut parallel to the rolling direction. Uniaxial tensile tests were conducted at room temperature using an Instron 8502 machine on sub-sized specimens with the gage dimensions of $15 \times 6 \times 1$ mm at an initial strain rate of 7×10^{-4} s^{-1}.

Microstructural examinations were performed on a JEOL JEM-2200FS transmission electron microscope (TEM) operated at 200 kV and a field emission gun Zeiss Sigma scanning electron microscope equipped with an electron backscatter diffraction (EBSD) device. Specimens for TEM were first ground to a thickness of 100 μm and then prepared using twin-jet

electropolishing at -15 °C in an electrolyte consisting by volume of 6% perchloric acid, 35% butanol and 59% water. Samples for EBSD scans were first mechanically polished using diamond suspension with an average size down to 1 μm and then chemically polished with a solution of H_2O_2 and OP-S (oxide polishing suspension from Struers, a colloidal silica suspension with a pH of 9.8 and a grain size of 0.04 μm). The EBSD scans were performed with a step size of 0.05 μm.

3. Results and discussion

Figure 1a reveals that the microstructure of the produced alloy consists of equiaxed β phase grains with the average size of ~30 µm. Nevertheless, the spots related to ω phase are evident in the selected area electron diffraction (SAED) pattern of the sample shown in Fig. 1b. This means that athermal ω phase is formed in the alloy upon quenching. The corresponding dark field image (Fig. 1c), derived from the ω spot marked by a circle in Fig. 1b, indicates that nano-sized (less than 10 nm) ω precipitates are homogeneously dispersed throughout the matrix.

Figure 2a shows the tensile stress-strain curve of the alloy. As seen, the alloy exhibits very high yield strength (YS) of 920 MPa and an excellent total elongation (EL) of 31%. Such a YS-EL combination is not common in conventional Ti alloys and has only been reported in Gum metals. According to Fig. 2a, the engineering stress-strain curve shows a small flow stress peak in the beginning of plastic deformation, which is followed by a long plateau-type flat plastic region. After the initial drop and following increase, the strain hardening rate is low and constant over the true strain range until about 18%, as shown by the insert in Fig. 2a. A yield point and low strain hardening along long elongation are the features similar to those typical in Gum metals [1, 23, 24]. Figure 2b shows EL versus YS for the present alloy in comparison to those of other published β Ti alloys [20, 23, 25-29]. All the alloys illustrated in Fig. 2b were solution treated

4

before testing at room temperature and had similar gauge dimensions. As seen for most of the alloys, the higher YS, the lower EL, while the present Ti-3873 alloy is an exception exhibiting high strength and elongation. Several strengthening mechanisms including solid solution, grain size and nano-sized ω precipitates may contribute to the high YS of the alloy. By assuming a same volume fraction and size of the ω phase in the present alloy and Gum metals, the higher YS of Ti-3873 is determined by its finer grain size (30 μm) compared to Gum metal (60-150 μm [23, 27]) and solid solution effect (i.e. chemical composition). According to the estimate of solid solution strengthening of alloying elements recently suggested by present authors [30], the YS of Ti-3873 is expected to be 790–990 MPa which is in agreement with the experimental observation.

The drop in the stress from the upper yield point to the lower yield strength level, from 920 MPa to ~900 MPa, is the similar yield point phenomenon at the beginning of plastic deformation as observed in several alloys, such as carbon steels [31], Cu-Zn [32], Al-Mg [33] and Ti alloys [1, 19, 20, 22]. Conventionally the yield point phenomenon is explained as a result from initial pinning of dislocations by solute atoms and rapid increase in the number of mobile dislocations after the release [34]. The yield point followed by discontinuous yielding (Lüders-strain without strain hardening) has also been detected in an Al-Mg-Li alloy in connection with precipitates [35] and in an ultrafine-grained Fe-C alloy with carbide particles [36]. Regarding Ti alloys, the coherent ω phase particles could prevent dislocation movement until the stress is capable to shear them [23]. However, some Ti alloys with a high fraction of the ω phase does not exhibit any yield point [23] and the yield point has also been observed in some Ti alloys without ω precipitates [37]. Therefore, it seems that there is not distinct connection between the ω precipitates and the existence of yield point. The yield point has also been reported in a Gum

metal with the chemical composition of Ti-12Ta-9Nb-3V-6Zr-1.5O (at.%) [1]. Lai et al. [23] have observed similar results in Ti-23Nb-0.7Ta-2Zr (at.%) alloy with 1.2 and 1.5 at.% of oxygen. They concluded that the occurrence of yield point is caused by oxygen atoms forming Cottrell-clouds on dislocations and thereby depends on the oxygen content. The yield point was present when the concentration of oxygen is higher than 1.2 at.%. However, the fact is that the yield point has also been observed in some Ti alloys with a low amount of oxygen [19, 20] and the faint yield point is visible in the stress-strain curve of the present alloy with the oxygen content of about 0.56 at.%. This indicates that the yield point can appear with low contents of oxygen depending on alloying system. Hence, the reason for the formation of the yield point remains unclear.

The true stress-strain curve of the present alloy exhibits the low strain hardening rate at a high flow stress level and large elongation. To identify the active deformation mechanism(s), the deformed microstructure of tensile tested specimens was examined using TEM. Numerous dislocations were observed in 10% strained sample, as shown in Fig. 3a. In agreement with previous studies in β Ti alloys reporting glissile dislocations with the a/2 <111> Burgers vector [4, 5, 18], the Burgers vector of long straight parallel dislocations, shown by arrows, was determined to be a/2 <111> based on the g.b=0 invisibility criterion. Although the slip planes of a/2 <111> dislocations can be {112} or {110} planes, the characterization of slip traces left by dislocations in some beta Ti alloys have indicated that these dislocations move preferentially on {112} type slip planes [23]. Some cross slip segments of dislocations were also observed as pointed out with arrows in Fig. 3b. This confirms the possibility of dislocation cross slip in the present alloy. Several straight dislocations are present inside a grain also in Fig. 3c. The straight dislocations were characterized to be mainly screw-type dislocations. It has been shown that the

velocity of screw segments of dislocations is lower than their non-screw segments leading to the presence of high density of straight screw dislocations [4]. Furthermore, Fig. 3c reveals intense dislocation multiplication during straining. Dislocations are initially pinned, and as a result of gliding they leave loops on behind (shown with arrows in Fig. 3c). The dislocation multiplication mechanism in Ti alloys based on the core pinning, as reported in previous studies [5, 18] is attributed to cross slip and its frequent occurrence leads to appearance of distinct slip bands. As seen in Fig. 3a, most of dislocations tend to remain on distinct narrow slip bands for dislocation glide. Figure 3d shows a dark field image of the deformed specimen recorded using the ω diffraction spot marked with a circle in the SAED pattern shown in the inset. Though that the SAED is similar to that of the annealed sample (Fig. 1b), these dark field images show a striking difference, for several bands are clearly visible in the deformed microstructure. These bands are essentially channels devoid of ω precipitates. This indicates that the ω phase has transformed back into the β phase as a result of deformation. Similar precipitate-free channels have been observed in other deformed ω-containing Ti alloys [23, 38] as well as irradiated metals and alloys [39, 40]. Recently, Lai et al. [23] demonstrated that due to the coherence existing in a certain slip system the ω particles can be sheared and the repeated passage of {1 1 2}<1 1 1> dislocations on {112}$_\beta$ planes promotes the transformation of ω into β and forms ω-free channels by the dislocation dissociation mechanism. This scenario also justifies our observations of {112} planes as preferred dislocations slip planes in Figs 3a and 3d.

The upper yield point value of 920 MPa obtained in the present alloy is much higher than the yield strength of the Gum metal [1, 23]. According to the true stress-strain curve shown in Fig. 2a, the true tensile strength is about 1100 MPa which is also much higher than that in Gum metals. In addition to the strength, the alloy shows an excellent total elongation of 31% (true

strain 27%). Recently, the present authors showed that Ti-3873 exhibits a high compressive ductility and good workability [21]. The inset in Fig. 2a shows the variation of strain hardening rate as a function of true strain. As seen, the alloy exhibits a low strain hardening rate (about 1000 MPa) which stays almost constant until a high strain level. As mentioned before, this low strain hardening range is similar to that in Gum metals [1, 23]. Lai et al. [23] suggested that the limited but positive SHR is responsible for the large elongation to fracture in the Ti–23Nb–0.7Ta–2Zr–1.52O alloy. Generally, the lack of strain hardening would lead to plastic instability and localization of plastic strain. To identify the factors affecting the strain hardening, more TEM micrographs were taken from the 10% tensile strained specimen. Two types of dislocation configuration were observed: I) dislocation channels, i.e. a high density of dislocations confined along narrow slip bands and II) intersecting structure of dislocation channels with each other or twins. According to Fig. 3e, the channels may traverse each other. In addition, very limited number of twins were observed in the microstructure of deformed samples. Figure 3f shows a twin with a high dislocation density. Twins, though in small numbers, were also observed after compressive deformation of this alloy [21]. Dislocation slip and channels may intersect with twin boundaries. Therefore, these interactions between the channels with each other, with twin boundaries and also dislocation loops within the channels can lead to strain hardening, although in a low amount.

It seems that at higher strains some further mechanism(s) are activated affecting the strain hardening behavior. To understand the underlying phenomenon, the microstructure of samples was investigated at the strain close to the start of local necking. Figures 4(a) and 4(b) show the EBSD maps of the tensile tested specimens after applying 20% nominal strain. The image quality and inverse pole figure maps reveal that in addition to the elongated grains, some thick

deformation bands are formed inside the grains which exhibit different orientations respect to the matrix. The variation of misorientation across one of the bands is plotted in Fig. 4c. As seen, the misorientation angle is below 30° indicating that these bands cannot be mechanical twins since the misorientation angle between the twin and matrix is about 50.7° in β Ti alloys [22]. In addition, some crystal rotations are observed inside the bands, as shown with arrows in Fig. 4c. Similar band structures have been observed during compressive deformation of the Ti-22.4Nb-0.73Ta-2Zr-1.34O (at.%) alloy [22]. Furuta et al. [41] also reported similar structures in a same alloy after 40% cold swaging. They showed that the misorientation angle between the band structures and matrix is in the range of 10–30° in agreement with our results. They argued that the bands are formed with a dislocation free mechanism. However since that these bands exhibit some crystallographic characteristics similar to the kink bands, Yang et al. [22] suggested that they are most probably kink bands. Referring to high activity of dislocations during straining, the latter theory is more acceptable for the present alloy. It has been shown that the formation of kink bands results in an enhanced ductility and workability [22]. The formation of kink bands locally accommodating deformation also leads to strain softening. To investigate large areas corresponding to the deformation bands, several micrographs were taken from the gauge length at different strains. Figure 5 shows the results for the tensile tested specimens after applying 5%, 10%, 15% and 20% nominal strain. A large number of band structures (shown with circles in Fig. 5) is observed in the microstructure of tensile tested samples and with increasing strain, the incidence of bands increases. Similar results have been reported by authors for Ti-4Al-7Mo-3V-3Cr [42]. It has been shown that the misorientation inside the grains increases with increasing strain and a considerable amount of deformation is accommodated by crystal rotation in the bands [42]. Therefore, it can be suggested that the formation of kink bands with a strain

9

softening mechanism occurs simultaneously with the interaction of dislocation channels with a strain hardening mechanism and result in low strain hardening but high ductility.

4. Conclusions

Deformation behavior of the beta Ti-2.9Al-7.9Mo-7V-3Cr-0.18O (wt. %) (Ti-3873) alloy during uniaxial tensile straining at room temperature was investigated. The alloy exhibits a high yield strength of 920 MPa with an excellent elongation to failure of 31%. Some specific deformation features such as yield point phenomenon and very low strain hardening were observed. The yield point may be attributed to the presence of oxygen and the omega precipitates in the alloy. Dislocations were found to confine to narrow omega-free slip bands during deformation. Two types of deformation mechanisms governing strain hardening and strain softening were identified. Dislocation loops within the channels and intersecting of slip bands and twins was supposed to lead to strain hardening. On the other hand, the formation of kink bands at higher strains with crystal rotation inside the grains caused strain softening, almost balancing the flow stress.

Data availability
The raw/processed data required to reproduce these findings cannot be shared at this time as the data also forms part of an ongoing study.

References

[1] T. Saito, T. Furuta, J.-H. Hwang, S. Kuramoto, K. Nishino, N. Suzuki, R. Chen, A. Yamada, K. Ito, Y. Seno, T. Nonaka, H. Ikehata, N. Nagasako, C. Iwamoto, Y. Ikuhara, T. Sakuma, Multifunctional alloys obtained via a dislocation-free plastic deformation mechanism, Sci. 300(5618) (2003), pp. 464-467.
[2] M.Y. Gutkin, T. Ishizaki, S. Kuramoto, I.A. Ovid'ko, N.V. Skiba, Giant faults in deformed gum metal, Int. J. Plas. 24(8) (2008), pp.1333-1359.
[3] T. Li, J.W. Morris, N. Nagasako, S. Kuramoto, D.C. Chrzan, Ideal engineering alloys, Phys. Rev. Lett. 98(10) (2007), 105503.

[4] M. Besse, P. Castany, T. Gloriant, Mechanisms of deformation in gum metal TNTZ-O and TNTZ titanium alloys: A comparative study on the oxygen influence, Acta Mater. 59(15) (2011), pp. 5982-5988.

[5] P. Castany, M. Besse, T. Gloriant, Dislocation mobility in gum metal β-titanium alloy studied via in situ transmission electron microscopy, Phys. Rev. B 84 (2011), 020201.

[6] H. Xing, J. Sun, Mechanical twinning and omega transition by ⟨111⟩ {112} shear in a metastable β titanium alloy, Appl. Phys. Lett. 93(3) (2008), 031908.

[7] R.J. Talling, R.J. Dashwood, M. Jackson, D. Dye, On the mechanism of superelasticity in Gum metal, Acta Mater. 57(4) (2009), pp. 1188-1198.

[8] J.W. Morris Jr, Y. Hanlumyuang, M. Sherburne, E. Withey, D.C. Chrzan, S. Kuramoto, Y. Hayashi, M. Hara, Anomalous transformation-induced deformation in ⟨110⟩ textured Gum Metal, Acta Mater. 58(9) (2010), pp. 3271-3280.

[9] M. Tane, T. Nakano, S. Kuramoto, M. Hara, M. Niinomi, N. Takesue, T. Yano, H. Nakajima, Low Young's modulus in Ti–Nb–Ta–Zr–O alloys: Cold working and oxygen effects, Acta Mater. 59(18) (2011), pp. 6975-6988.

[10] E.A. Withey, A.M. Minor, D.C. Chrzan, J.W. Morris, S. Kuramoto, The deformation of Gum Metal through in situ compression of nanopillars, Acta Mater. 58(7) (2010), pp. 2652-2665.

[11] S. Hanada, O. Izumi, Transmission electron microscopic observations of mechanical twinning in metastable β titanium alloys, Metall. Trans. A 17 (1986), pp. 1409-1420.

[12] H.Y. Kim, Y. Ikehara, J.I. Kim, H. Hosoda, S. Miyazaki, Martensitic transformation, shape memory effect and superelasticity of Ti–Nb binary alloys, Acta Mater. 54(9) (2006), pp. 2419-2429.

[13] Y.L. Hao, S.J. Li, S.Y. Sun, C.Y. Zheng, R. Yang, Elastic deformation behaviour of Ti–24Nb–4Zr–7.9Sn for biomedical applications, Acta Bio. 3(2) (2007), pp. 277-286.

[14] T. Inamura, Y. Yamamoto, H. Hosoda, H.Y. Kim, S. Miyazaki, Crystallographic orientation and stress-amplitude dependence of damping in the martensite phase in textured Ti–Nb–Al shape memory alloy, Acta Mater. 58(7) (2010), pp. 2535-2544.

[15] X. Min, X. Chen, S. Emura, K. Tsuchiya, Mechanism of twinning-induced plasticity in β-type Ti–15Mo alloy, Scr. Mater. 69(5) (2013), pp. 393-396.

[16] M.J. Lai, C.C. Tasan, D. Raabe, On the mechanism of {332} twinning in metastable β titanium alloys, Acta Mater. 111 (2016), pp. 173-186.

[17] E. Bertrand, P. Castany, I. Péron, T. Gloriant, Twinning system selection in a metastable β-titanium alloy by Schmid factor analysis, Scr. Mater. 64(12) (2011), pp. 1110-1113.

[18] P. Castany, M. Besse, T. Gloriant, In situ TEM study of dislocation slip in a metastable β titanium alloy, Scr. Mater. 66(6) (2012), pp. 371-373.

[19] X.H. Min, S. Emura, T. Nishimura, K. Tsuchiya, K. Tsuzaki, Microstructure, tensile deformation mode and crevice corrosion resistance in Ti–10Mo–xFe alloys, Mater. Sci. Eng. A 527(21-22) (2010), pp. 5499-5506.

[20] X.H. Min, S. Emura, N. Sekido, T. Nishimura, K. Tsuchiya, K. Tsuzaki, Effects of Fe addition on tensile deformation mode and crevice corrosion resistance in Ti–15Mo alloy, Mater. Sci. Eng. A 527(10-11) (2010), pp. 2693-2701.

[21] S. Sadeghpour, S.M. Abbasi, M. Morakabati, A. Kisko, L.P. Karjalainen, D.A. Porter, On the compressive deformation behavior of new beta titanium alloys designed by d-electron method, J. Alloy. Compd. 746 (2018), pp. 206-217.

[22] Y. Yang, S.Q. Wu, G.P. Li, Y.L. Li, Y.F. Lu, K. Yang, P. Ge, Evolution of deformation mechanisms of Ti–22.4Nb–0.73Ta–2Zr–1.34O alloy during straining, Acta Mater. 58(7) (2010), pp. 2778-2787.

[23] M.J. Lai, C.C. Tasan, D. Raabe, Deformation mechanism of ω-enriched Ti–Nb-based gum metal: Dislocation channeling and deformation induced ω–β transformation, Acta Mater. 100 (2015), pp. 290-300.

[24] E. Plancher, C.C. Tasan, S. Sandloebes, D. Raabe, On dislocation involvement in Ti–Nb gum metal plasticity, Scr. Mater. 68(10) (2013), pp. 805-808.

[25] C.H. Wang, A.M. Russell, G.H. Cao, A semi-empirical approach to the prediction of deformation behaviors of β-Ti alloys, Scr. Mater. 158 (2019), pp. 62-65.

[26] F. Sun, J.Y. Zhang, M. Marteleur, T. Gloriant, P. Vermaut, D. Laillé, P. Castany, C. Curfs, P.J. Jacques, F. Prima, Investigation of early stage deformation mechanisms in a metastable β titanium alloy showing combined twinning-induced plasticity and transformation-induced plasticity effects, Acta Mater. 61(17) (2013), 6406-6417.

[27] J.L. Zhang, C.C. Tasan, M.J. Lai, D. Yan, D. Raabe, Partial recrystallization of gum metal to achieve enhanced strength and ductility, Acta Mater. 135 (2017), pp. 400-410.

[28] S.L. Nyakana, J.C. Fanning, R.R. Boyer, Quick reference guide for β titanium alloys in the 00s, J. Mater. Eng. Perf. 14(6) (2005), pp. 799-811.

[29] J. Gao, Y. Huang, D. Guan, A.J. Knowles, L. Ma, D. Dye, W.M. Rainforth, Deformation mechanisms in a metastable beta titanium twinning induced plasticity alloy with high yield strength and high strain hardening rate, Acta Mater. 152 (2018), pp. 301-314.

[30] S. Sadeghpour, S.M. Abbasi, M. Morakabati, A. Kisko, L.P. Karjalainen, D.A. Porter, A new multi-element beta titanium alloy with a high yield strength exhibiting transformation and twinning induced plasticity effects, Scr. Mater. 145 (2018), pp. 104-108.

[31] G. Ananthakrishna, Current theoretical approaches to collective behavior of dislocations, Phys. Rep. 440(4) (2007), pp. 113-259.

[32] G.W. Ardley, A.H. Cottrell, Yield points in brass crystals, Proceedings of the Royal Society of London. Series A 219(1138) (1953), pp. 328-340.

[33] H. Aboulfadl, J. Deges, P. Choi, D. Raabe, Dynamic strain aging studied at the atomic scale, Acta Mater. 86 (2015), pp. 34-42.

[34] S.D. Mesarovic, Dynamic strain aging and plastic instabilities, J. Mech. Phys. Solid. 43(5) (1995), pp. 671-700.

[35] Z.C. Wang, P.B. Prangnell, Microstructure refinement and mechanical properties of severely deformed Al–Mg–Li alloys, Mater. Sci. Eng. A 328(1) (2002), pp. 87-97.

[36] T. Lee, C.H. Park, D.-L. Lee, C.S. Lee, Enhancing tensile properties of ultrafine-grained medium-carbon steel utilizing fine carbides, Mater. Sci. Eng. A 528(21) (2011), pp. 6558-6564.

[37] F. Geng, M. Niinomi, M. Nakai, Observation of yielding and strain hardening in a titanium alloy having high oxygen content, Mater. Sci.Eng. A 528(16-17) (2011), pp. 5435-5445.

[38] S. Banerjee, U.M. Naik, Plastic instability in an omega forming Ti-15% Mo alloy, Acta Mater. 44(9) (1996), pp. 3667-3677.

[39] T. Diaz de la Rubia, H.M. Zbib, T.A. Khraishi, B.D. Wirth, M. Victoria, M.J. Caturla, Multiscale modelling of plastic flow localization in irradiated materials, Nat. 406 (2000), pp. 871-874.

[40] D. Kiener, P. Hosemann, S.A. Maloy, A.M. Minor, In situ nanocompression testing of irradiated copper, Nat. Mater. 10 (2011), pp. 608-613.

[41] T. Furuta, S. Kuramoto, J. Hwang, K. Nishino, T. Saito, Elastic deformation behavior of multi-functional Ti–Nb–Ta–Zr–O alloys, Mater. Trans. 46 (2005), pp.3001-3007.
[42] S. Sadeghpour, S.M. Abbasi, M. Morakabati, L.P. Karjalainen, D.A. Porter, Effect of cold rolling and subsequent annealing on grain refinement of a beta titanium alloy showing stress-induced martensitic transformation, Mater. Sci. Eng. A 731 (2018), pp. 465-478.
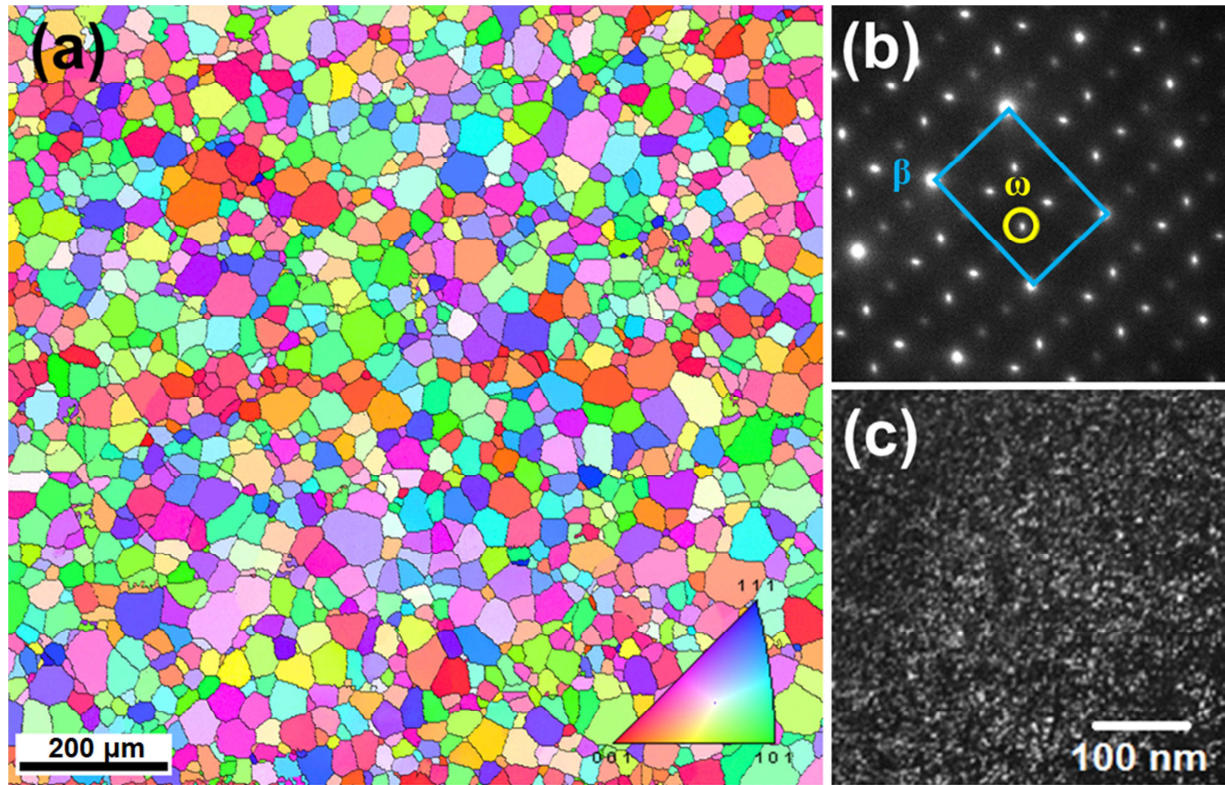
Figure Captions:

Fig. 1. (a) EBSD inverse pole figure map of the annealed Ti-3873 alloy overlaid by grain boundaries indicated by black (>15°) lines. (b) SAED pattern along $[110]_\beta$ zone axis corresponding to (b). (c) Dark-field TEM micrograph taken from the diffraction spot indicated by a circle in (b) showing athermal ω precipitates.

Fig. 2. (a) Tensile stress-strain curves of the Ti-3873 alloy. The inset shows the corresponding strain hardening rate (SHR) as a function of true strain. (b) Yield strength (YS) vs. total elongation (EL) scatter plot of the studied alloy in comparison to literature data for some beta Ti alloys [20, 23, 25-29].
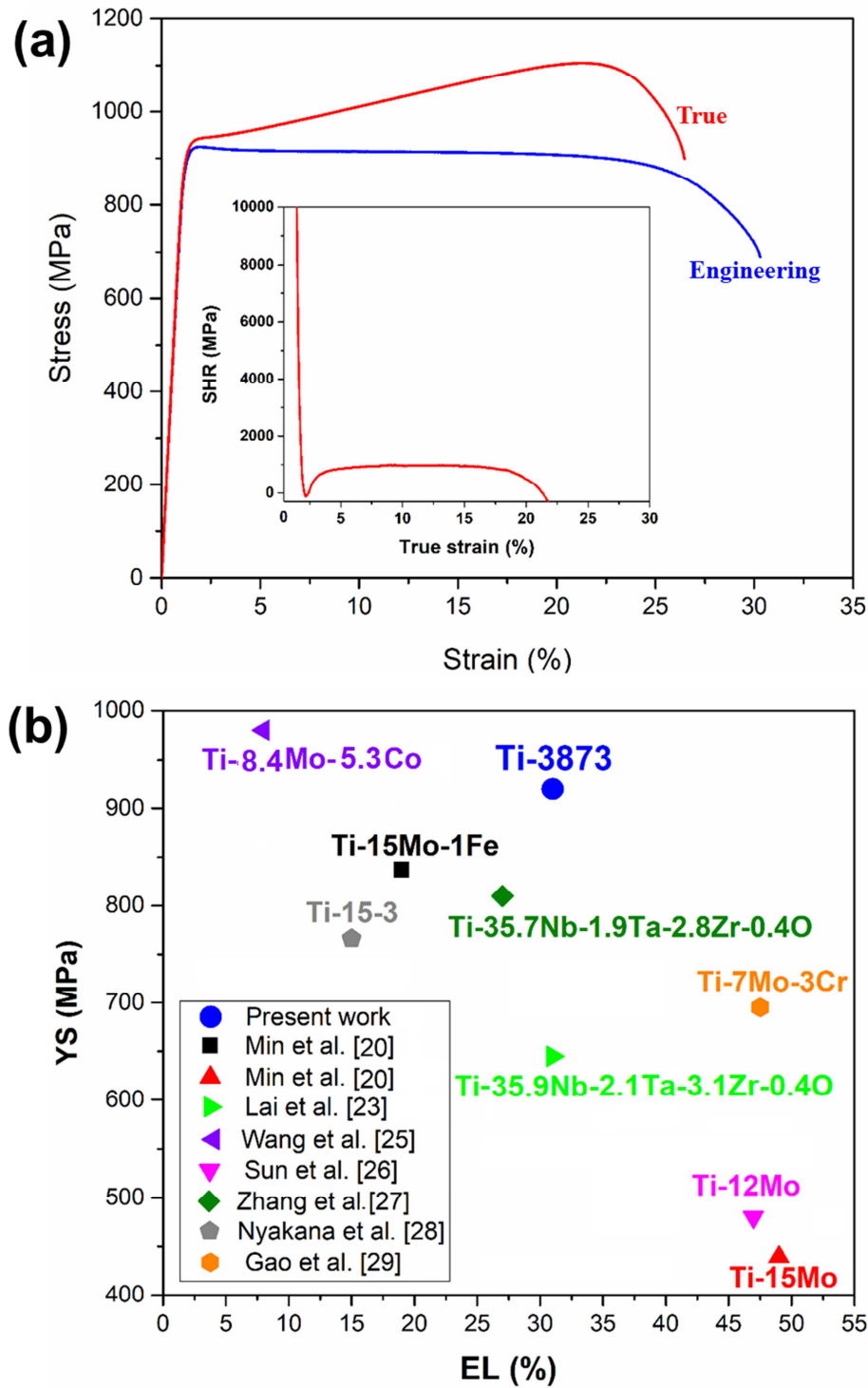
Fig. 3. STEM micrographs of the 10% strained specimen showing (a) formation of dislocation channels, (b) higher magnification of the area marked by rectangle in (a) showing dislocation cross slip, (c) straight screw dislocations and dislocation loop formation and expansion. (d) Dark field TEM micrograph taken from ω diffraction spots marked in the $[110]_\beta$ SAED pattern shown in the inset, (e) Cross-hatched dislocation channels, (f) Several dislocation channels intersecting each other and twin boundaries.

Fig. 4. EBSD maps of Ti-3873 after 20% of tensile strain. (a) Image quality and (b) Inverse pole figure maps. (c) Misorientation along the AB arrow shown in (b).
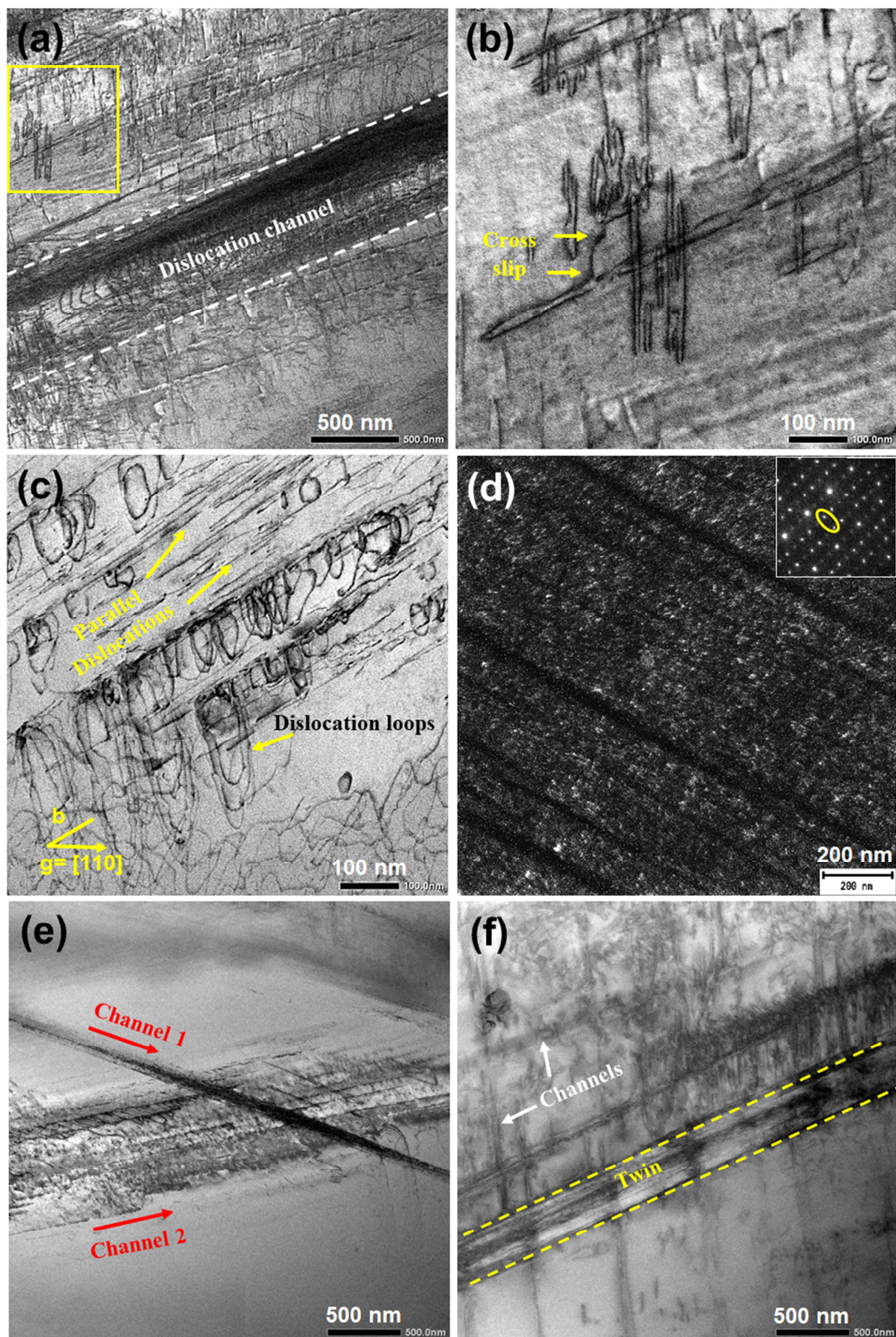
Fig. 5. Scanning electron micrographs of Ti-3873 after a)5%, b)10%, c) 15% and d)20% of tensile strain.
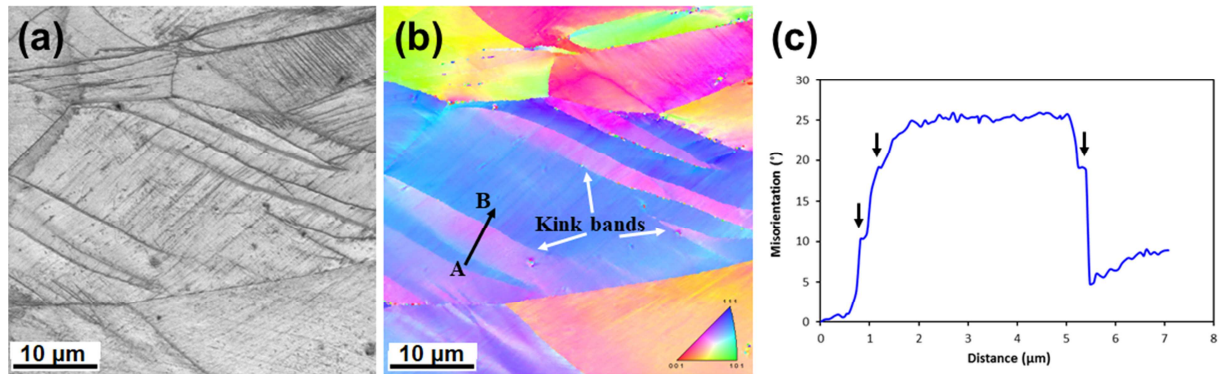
13

Fig. 1. (a) EBSD inverse pole figure map of the annealed Ti-3873 alloy overlaid by grain boundaries indicated by black (>15°) lines. (b) SAED pattern along $[110]_\beta$ zone axis corresponding to (b). (c) Dark-field TEM micrograph taken from the diffraction spot indicated by a circle in (b) showing athermal ω precipitates.
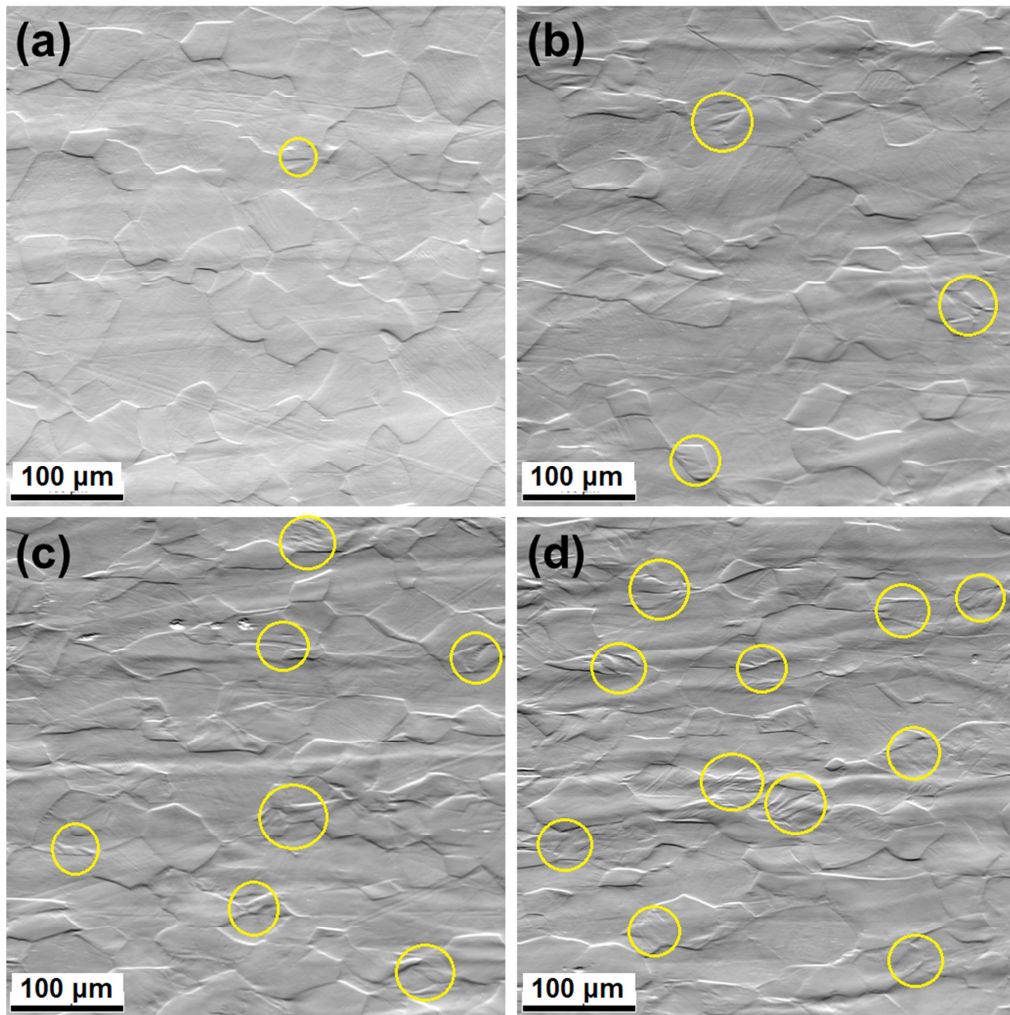
Fig. 2. (a) Tensile stress-strain curves of the Ti-3873 alloy. The inset shows the corresponding strain hardening rate (SHR) as a function of true strain. (b) Engineering yield strength (YS) vs. total elongation (EL) scatter plot of the studied alloy in comparison to literature data for some beta Ti alloys [20, 23, 25-29].

(a) Dislocation channel — 500 nm

(b) Cross slip — 100 nm

(c) Parallel Dislocations, Dislocation loops, b, g= [110] — 100 nm

(d) 200 nm

(e) Channel 1, Channel 2 — 500 nm

(f) Channels, Twin — 500 nm

Fig. 3. STEM micrographs of the 10% strained specimen showing (a) formation of dislocation channels, (b) higher magnification of the area marked by rectangle in (a) showing dislocation cross slip, (c) straight screw dislocations and dislocation loop formation and expansion. (d) Dark field TEM micrograph taken from ω diffraction spots marked in the $[110]_\beta$ SAED pattern shown in the inset, (e) Cross-hatched dislocation channels, (f) Several dislocation channels intersecting each other and twin boundaries.

Fig. 4. EBSD maps of Ti-3873 after 20% of tensile strain. (a) Image quality and (b) Inverse pole figure maps. (c) Misorientation along the AB arrow shown in (b).

Fig. 5. Scanning electron micrographs of Ti-3873 after a)5%, b)10%, c) 15% and d)20% of tensile strain.

Highlights

- The alloy of Ti-3873 exhibits a high YS of 920 MPa with an excellent EL of 31%.

- Two types of mechanisms governing strain hardening and softening were identified.

- Dislocation channeling and kink band formation lead to a high ductility.

- The joint strain hardening and softening results in a plateau stress-strain curve.